1

Cutting Dynamics and Machining Instability

Material removal – as the most significant operation in manufacturing industry – is facing the ever-increasing challenge of increasing proficiency at the micro and nano scale levels of high-speed manufacturing. Fabrication of submicron size three-dimensional features and freeform surfaces demands unprecedented performance in accuracy, precision, and productivity. Meeting the requirements for significantly improved quality and efficiency, however, are contingent upon the optimal design of the machine-tools on which machining is performed. Modern day precision machine-tool configurations are in general an integration of several essential components including process measurement and control, power and drive, tooling and fixture, and the structural frame that provides stiffness and stability. As dynamic instability is inherently prominent and particularly damaging in high-speed precision cutting, *design for dynamics* is favored for the design of precision machine tool systems [1]. This approach employs computer-based analysis and design tools to optimize the dynamic performance of machine-tool design at the system level. It is largely driven by a critical piece of information – the vibration of the machine-tool. Due to the large set of parameters that affect cutting vibrations, such as regenerative effects, tool nonlinearity, cutting intermittency, discontinuous frictional excitation, and environmental noise, among many others, the effectiveness of the approach commands that the dynamics of machining be completely established throughout the entire process.

This book explores the fundamentals of cutting dynamics to the formulation and development of an innovative control methodology. The coupling, interaction, and evolution of different cutting states are studied so as to identify the underlying critical parameters that can be controlled to negate machining instability and enable better machine-tool design for precision micro and nano manufacturing.

The main features that contribute to the robust control of cutting instability are: (1) comprehension of the underlying dynamics of cutting and interruptions in cutting motions, (2) operation of the machine-tool system over a broad range of operating conditions with

Control of Cutting Vibration and Machining Instability: A Time-Frequency Approach for Precision, Micro and Nano Machining, First Edition. C. Steve Suh and Meng-Kun Liu.

minimal vibration, such as high-speed operation to achieve a high-quality finish of the machined surface, (3) an increased rate of production to maximize profit and minimize operating and maintenance costs, (4) concentration on the apparent discontinuities that allows the nature of the complex machine-tool system motions to be fully established. The application of simultaneous time-frequency nonlinear control to mitigate complex intermittent cutting is both novel and unique. The impact on the area of material removal processes is in the mitigation of cutting instability and chaotic chattering motion induced by frictional and tool nonlinearity, and (5) development of concepts for cutting instability control and machine-tool design applicable to high-speed cutting processes.

1.1 Instability in Turning Operation

We start the book with a comprehensive investigation on machining instability by employing a three-dimensional turning model [2, 3, 4, 5] that addresses the concerns that (1) cutting dynamic models developed to date all fall short of grasping the underlying dynamics of turning operation and (2) stability charts developed using the models are inadequate to identify the true stability regions. The specific objective of the study is to establish the proper interpretation of cutting instability so as to establish the knowledge base for cutting instability control.

The complex machining model describes the coupled tool–workpiece dynamics subject to nonlinear regenerative cutting forces, instantaneous depth-of-cut, and workpiece whirling due to material imbalance. In the model the workpiece is considered a system of three rotor sections – namely, unmachined, being machined, and machined – connected by a flexible shaft, thus enabling the motion of the workpiece relative to the tool and tool motion relative to the machining surface to be three-dimensionally established as functions of spindle speed, depth-of-cut, rate of material removal, and whirling. Figure 1.1 shows the configuration of the tool engaging the section that is being cut where the deviation of the geometric center from the center of mass constitutes the eccentricity that characterizes workpiece whirling. Using the model a rich set of nonlinear behaviors of both the tool and workpiece – including period-doubling bifurcation and chaos signifying the extent of machining instability at various depth-of-cuts – was observed. Results presented therein agree favorably with physical

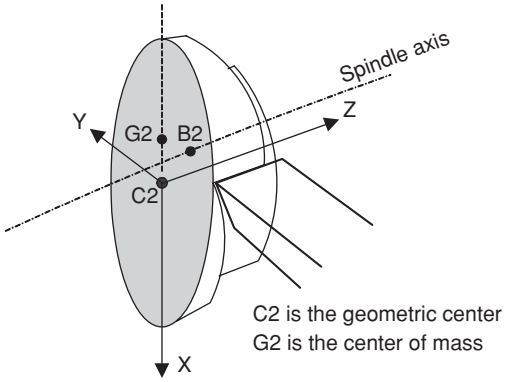

Figure 1.1 Configuration of the section that is being machined

experiments reported in the literature. It is found that at, and up to, certain ranges of depth-of-cuts, whirling is a non-negligible part of the fundamental characteristics of the machining dynamics. Contrary to common belief, whirling is found to have an insignificant impact on tool motions. The efforts documented in [2, 3, 4, 5] also show that the linearized turning model underestimates tool vibrations in the time domain and overestimates system behaviors in the frequency domain; whereas the nonlinear model agrees with the physical results reported in the literature in describing machining stability and chatter. The coupled workpiece–tool vibrations described by the nonlinear model are more pragmatic than the linearized counterpart in revealing the true machining state of motion. The model also reveals in the qualitative sense the broadband behavior of the tool natural frequency associated with unstable situations. Vibration amplitudes obtained using the linearized model, however, are diverging at certain depth-of-cuts (DOCs) without the commonly observed randomness in oscillation. Moreover, the linearized model deems instability at low DOCs and predicts a bifurcated state of unstable motion that is described as chaotic using physical data. Many important insights are gained using the model, including the fact that if the underlying dynamics of machining is to be established, and stability limits to be precisely identified, linearization of the nonlinear model is not advisable.

1.1.1 Impact of Coupled Whirling and Tool Geometry on Machining

In addition to speed, feed rate, and DOC that affect material removal rate (MRR) and determine cutting force and hence power consumption, tool geometry is also one of the prominent parameters that impacts machining productivity. Surface roughness, chip formation changes, and chip flow angle are also affected by tool geometry. Even though chip flow angle is related to tool angles, chip flow angle is a function only of DOC. Figure 1.2 gives a view of the rake angle, α, while undergoing cutting action. Tool rake angle determines the flow of the newly formed chip. Usually the angle is between $+5^\circ$ and -5°. To compare with the experimental result reported in [6], a constant spindle speed $\Omega = 1250$ rpm, a constant chip width $t_0 = 0.0965$ mm, and an eccentricity $\varepsilon_1 = 0.2$ mm are considered along with several different DOCs including DOC $= 1.62$ mm and 2.49 mm. The workpiece considered is a 4140 steel bar of 0.25 m length (l_0) and $r_3 = 20.095$ mm radius of the machined section. The starting location of the carbide tool is set at 0.15 m from the chuck. There are three types of plots in the figures found in the sections that follow. The top rows plot time histories, whereas the middle rows give their corresponding time-frequency responses obtained using instantaneous frequency (which will be covered in great detail in Chapter 4). The last rows show the Lyapunov spectra where the largest Lyapunov exponents are shown. Instantaneous frequency is employed to realize subtle features characteristic of machining instability.

Positive rake makes the tool sharp, but it also weakens the tool compared with negative rake. Negative rake is better for rough cutting. The selection of tool geometry depends on the particular workpiece and tool materials being considered. To establish that tool angle does have significant effects on cutting stability, two sets of tool geometries are used to determine the cutting force in the following. Their values are given in Table 1.1. Both sets are taken from the tool inserts that were used in the experiments reported in [6]. Since DOC considered in the numerical study is less than 1 mm and can be considered as non-rough cutting, rake angles are taken as positive for all cases. Note that negative rake is better for roughing. Three

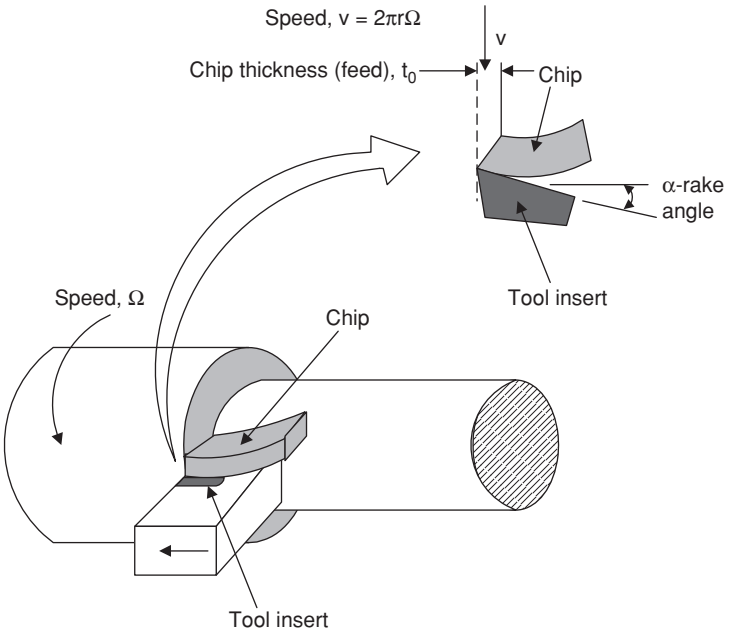

Figure 1.2 Cutting action with tool rake angle

DOCs (0.9 mm, 0.75 mm, and 0.5 mm) are used with a 1250 rpm spindle speed and a feed of 0.0965 mm per revolution in the study.

Except for Figures 1.6 and 1.7, all figures in Figures 1.3–1.8 give time responses, instantaneous frequency responses between 3 to 5 sec, and the corresponding Lyapunov spectra. X-direction system responses are examined to demonstrate workpiece behaviors, and Z-direction responses are analyzed to investigate tool motions. See also Figure 1.1 for the coordinates defined for the being-machined section. Plots in the right column correspond to Set #1 tool geometry conditions and the left column corresponds to Set #2 tool angles. In Figure 1.3, the X-direction vibration amplitude of Set #2 tool geometry is seen to be twice that of Set #1. However, their frequency domain behaviors are similar with a workpiece natural frequency at 3270 Hz and a whirling frequency at 20.8 Hz. Set #2 shows two more frequencies, one near the tool natural frequency at 425 Hz and another at 250 Hz, which disappears after 3.9 s. Set #1 has only one more tool-excited frequency. The frequency can be seen to decrease from 580 Hz to 460 Hz within 2 seconds, implying that tool geometry is a non-negligible parameter affecting workpiece stability.

Table 1.1 Tool angles

Set Number	Side cutting edge angle	Rake angle	Inclination angle
1	45°	3.55°	3.55°
2	15°	5°	0°

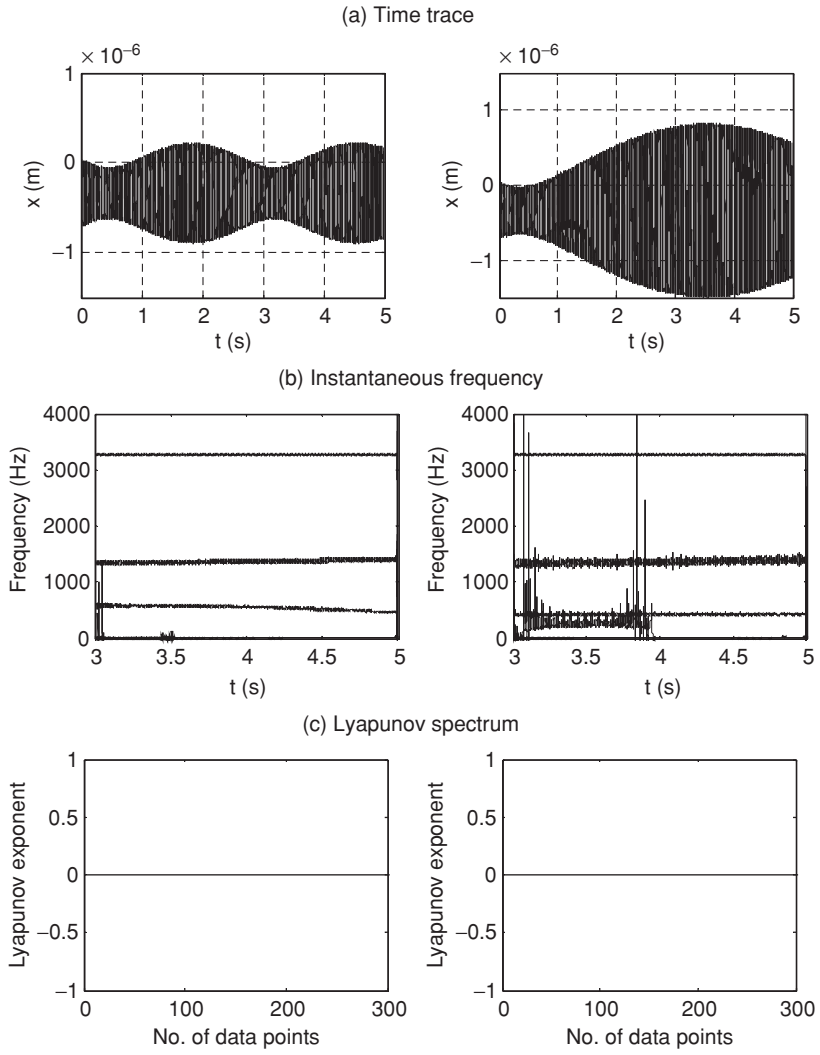

Figure 1.3 X-direction time responses, corresponding instantaneous frequency and Lyapunov spectra for Set #1(left) and Set #2 (right) for DOC = 0.90 mm at $\Omega = 1250$ rpm

When DOC is decreased to 0.75 mm in Figure 1.4, there are still differences in vibration amplitudes. With the reduction of its diameter, the workpiece natural frequency decreases to 3250 Hz. While whirling frequency remains the same, a 900 Hz component of a wide 500 Hz bandwidth dominates in both systems. It can be seen in Set #2 that a bifurcation of the tool-excited natural frequency at 425 Hz diminishes after 4.8 seconds. On the other hand, Set #1 does not have a bifurcation. It has a frequency component increase from 250 to 400 Hz. The frequency components then disappear afterward. Both Lyapunov spectra fluctuate near zero, thus leaving a question over whether the systems are exactly stable. Further deceasing DOC

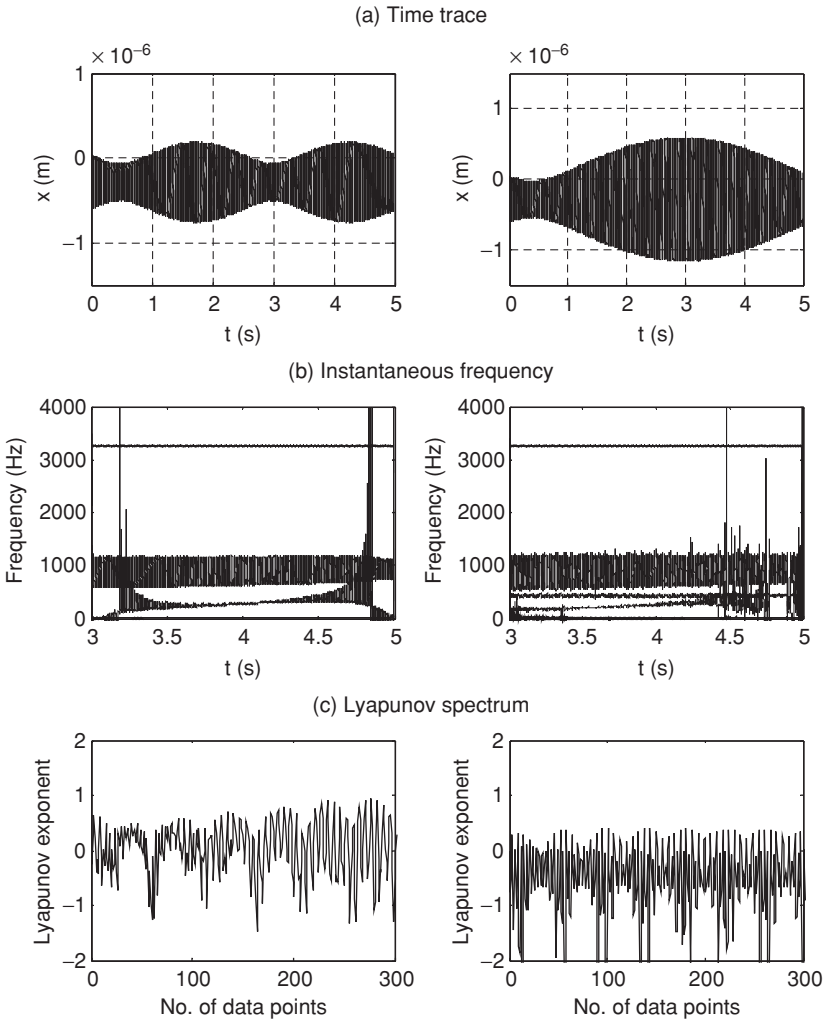

Figure 1.4 X-direction time responses, corresponding instantaneous frequency and Lyapunov spectra for Set #1(left) and Set #2 (right) for DOC = 0.75 mm at $\Omega = 1250$ rpm

to 0.5 mm in Figure 1.5 means both systems show an unstable situation marked by positive Lyapunov exponents.

The relatively large force fluctuation seen in Figure 1.6 explains the large vibration amplitudes seen for the tool geometry Set #2. Forces of large fluctuation push the workpiece to deflect more. It is interesting to note that, even though tool geometry variations are supposed to affect the cutting force, X-direction force amplitudes are almost identical for both tool geometry sets.

Effects of tool geometry can be seen in the Y- and Z-direction force components in Figure 1.7. While Y-direction forces for Set #2 are less than those of Set #1, Set #2 Z-direction forces are

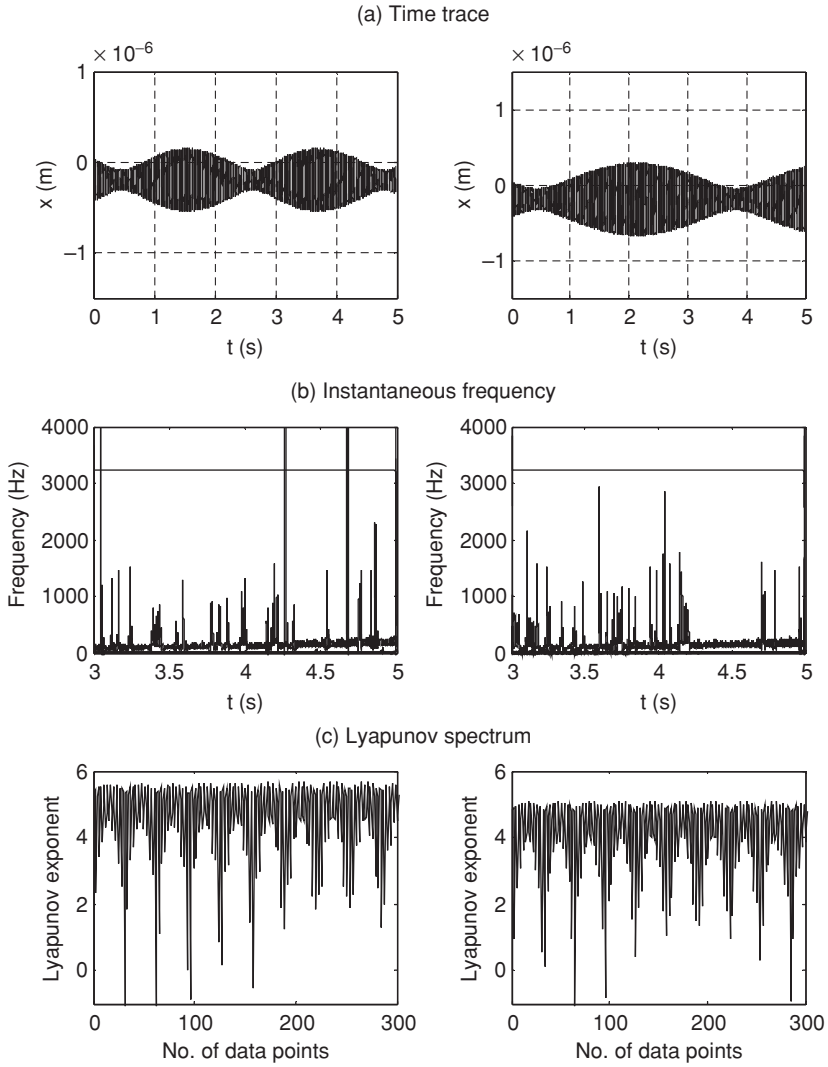

Figure 1.5 X-direction time responses, corresponding instantaneous frequency and Lyapunov spectra for Set #1(left) and Set #2 (right) for DOC = 0.50 mm at $\Omega = 1250$ rpm

much higher than those of Set #1. In all plots, it is seen that force responses associated with Set #1 tool geometry fluctuate less compared with those of Set #2. Tool dynamical motions for DOC = 0.9 mm, 0.75 mm, and 0.5mm are also considered. Even though force fluctuations and vibration amplitudes are both prominent, Set #2 is relatively more stable. Of the three DOCs considered, two behave dissimilarly. In all three cases, the vibration history of Set #1 has amplitudes that are of nanometers in scale. On the other hand, Set #2 vibrates with amplitudes that are a few microns for DOC = 0.9 mm and 0.75 mm, and several nanometers for DOC = 0.5 mm. Unlike Set #1, all Lyapunov spectra for Set #2 are evidence of a stable state of dynamic

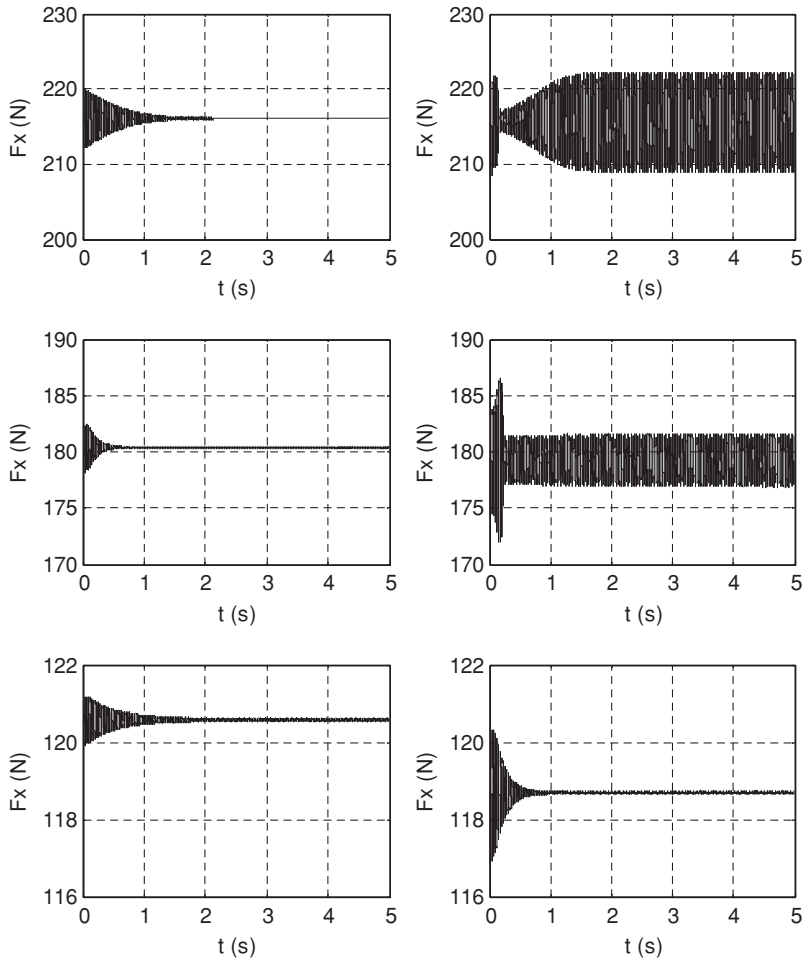

Figure 1.6 Forces in X- direction for Set #1(left) and Set #2 (right) for DOC = 0.90 mm (top), DOC = 0.75 mm (middle), and DOC = 0.50 mm (bottom) at $\Omega = 1250$ rpm

response. Though it has positive Lyapunov exponents, Set #2 shows instability for the DOC = 0.9 mm and 0.5 mm cases. IF plots for DOC = 0.9 mm in Figure 1.8 confirm that the Set #1 response is broadband and thus unstable, and Set #2 is stable with a clean spectrum. Although the Lyapunov spectrum indicates a stable state of tool motion for Set #1 at DOC = 0.75 mm, the corresponding instantaneous frequency suggests otherwise. The instantaneous frequency plot for Set #2 at DOC = 0.5 mm also contradicts the Lyapunov spectrum (not shown). A detailed review of the individual instantaneous frequency mono-components reveals that the frequency at 3240 Hz has bifurcated three times. Thus, it is in a highly bifurcated state.

The effects of tool geometry on cutting dynamics and its impact on surface finishing investigated above generate a few observations. The manufacturing industry has long learned to employ tool inserts with complex geometry to achieve better product surface finish. However,

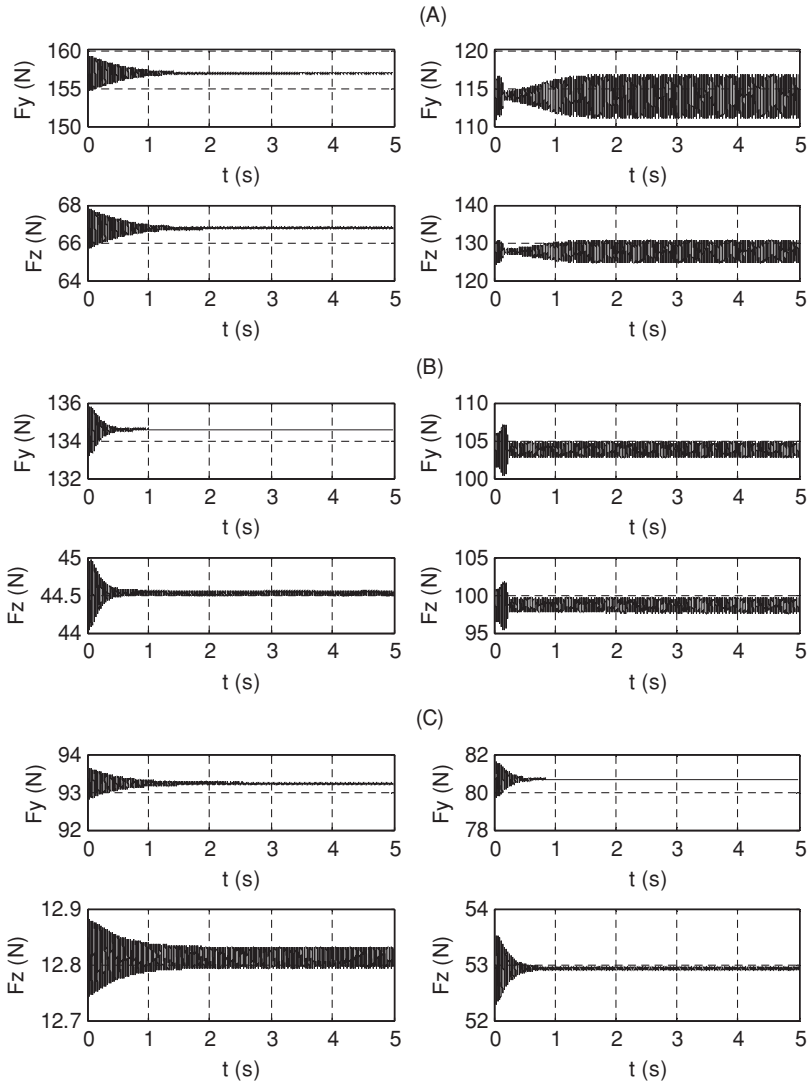

Figure 1.7 Forces in Y- and Z-direction for Set #1 (left) and Set #2 (right) for DOC = 0.90 mm (A), DOC = 0.75 mm (B), and DOC = 0.50 mm (C) at $\Omega = 1250$ rpm

most models developed for understanding machining dynamics and cutting stability ignore the various effects attributable to tool geometry. One of the reasons for this is the fact that 1D machining modeling is infeasible for incorporating various tool angles that are inherently 3D. Numerical experiments presented suggest that neglecting tool geometry is improbable. It was observed that variations in tool geometry can significantly impact cutting stability. A machining process can be unstable for a particular DOC using one set of tool geometry and become stable through careful selection of proper tool inserts with a different set of tool

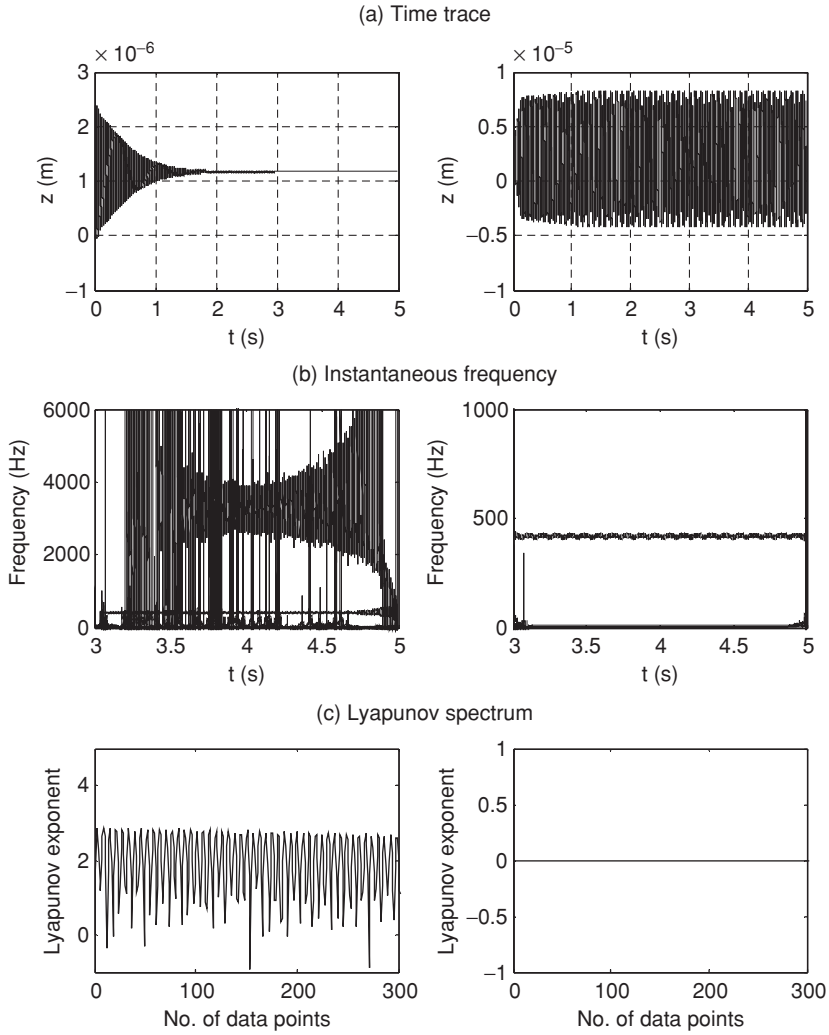

Figure 1.8 Z-direction time responses (tool vibrations), corresponding instantaneous frequency and Lyapunov spectra for Set #1 (left) and Set #2 (right) for DOC = 0.90 mm at $\Omega = 1250$ rpm

geometry at the same DOC. This raises the question over whether true dynamic stability can be identified without considering tool geometry. Thus, it is essential that tool geometry is also considered in modeling 3D turning operations.

1.2 Cutting Stability

The dynamic model is simulated using four different spindle speeds and several depth-of-cuts. Results presented in this section are only for DOC = 1.62 mm with a 0.0965 mm chip thickness.

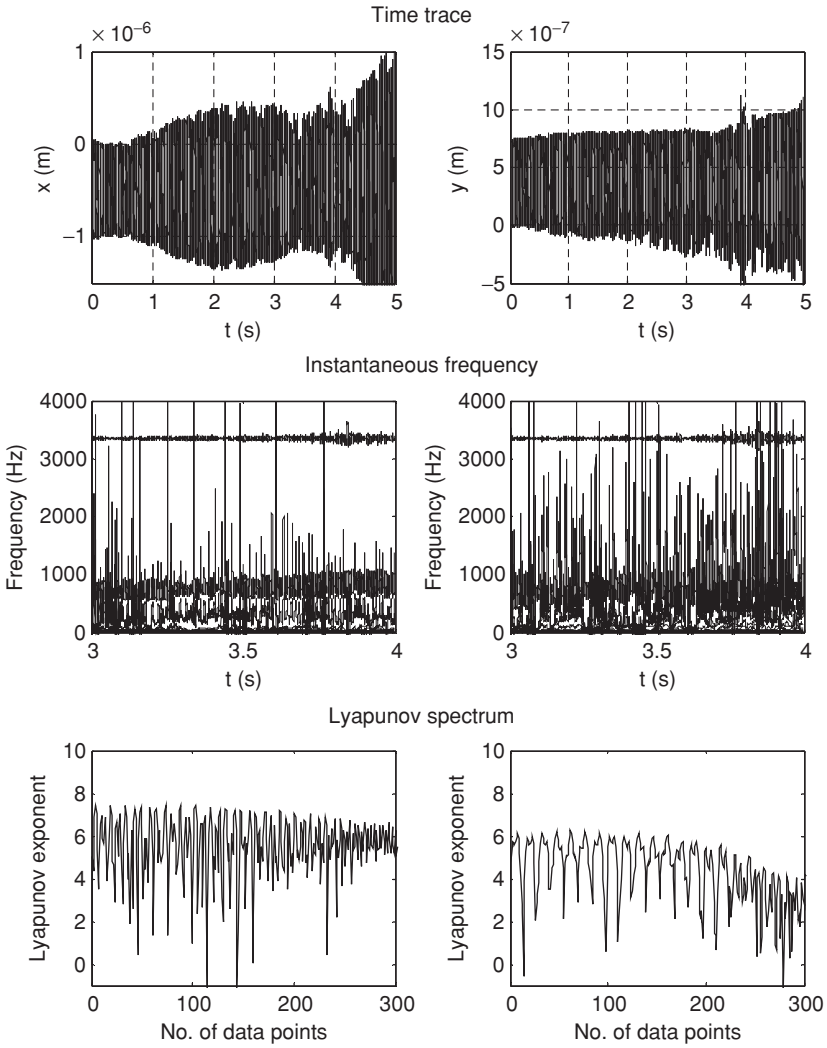

Figure 1.9 X-(left) and Y-(right) direction workpiece responses for DOC = 1.62 mm at $\Omega = 750$ rpm

In what immediately follows, we consider the time responses of the workpiece and the tool. Two spindle speeds, 750 rpm and 1000 rpm, are considered that correspond to the same DOC at 1.62 mm. Vibrations in all directions in Figure 1.9 and 1.10 seem random and the positive Lyapunov spectra indicate chaos. These are accompanied by broadband instantaneous frequency spectra. When the speed is increased to 1000 rpm, it can be seen in Figures 1.11 and 1.12 that both the workpiece and tool responses are remarkably stable. The time traces are periodic and the Lyapunov spectra are zero, implying that future vibrations can be predicted. Moreover, the instantaneous frequency plots show only three major frequencies

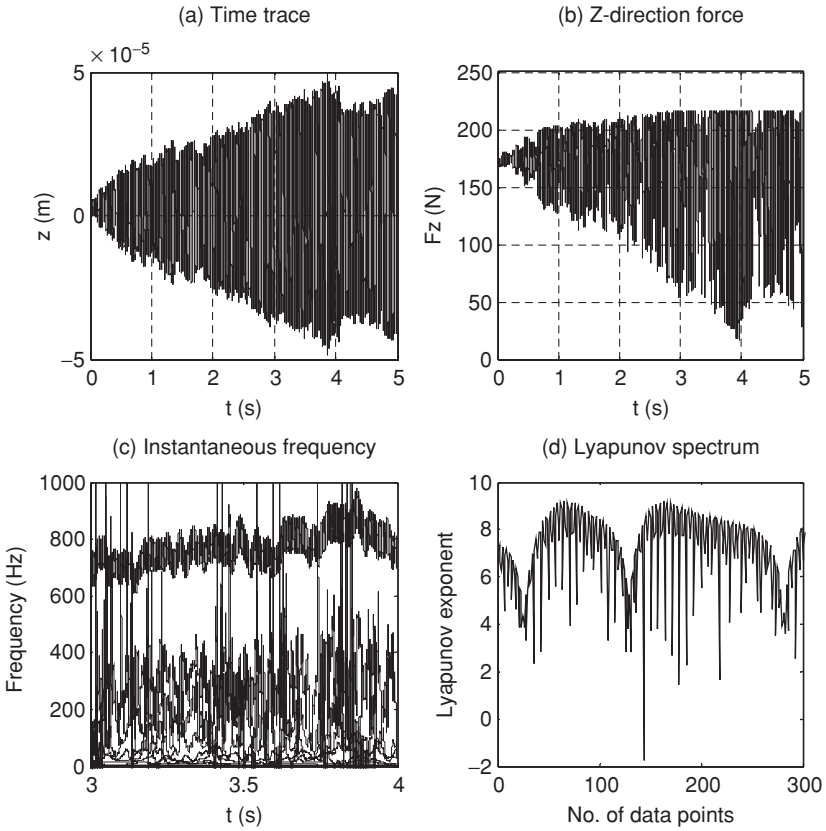

Figure 1.10 Z-direction tool behavior for DOC = 1.62 mm at Ω = 750 rpm

that do not bifurcate. These frequencies are: workpiece natural frequency at 3343 Hz, tool natural frequency at 425 Hz, and whirling frequency at 16.67 Hz.

Even though the workpiece is excited by the tool natural frequency subject to the action of cutting force components, the tool is not excited by the workpiece natural frequency. These are very important observations made with regard to the two different spindle speeds. Although physically engaged with the workpiece, however, the dynamics that governs the tool response is distinctively different from that of the workpiece's. This has a significant implication for the interpretation of cutting stability and the judging and characterizing of chatter. Simply put, machining chatter could be due to not just the cutting tool but also the workpiece.

1.3 Margin of Stability and Instability

The stable–unstable margins for rough turning at large DOCs are found for four different speeds at 750 rpm, 1000 rpm, 1250 rpm, and 1500 rpm. Workpiece and tool vibration responses of the cutting model system that correspond to stable DOCs and unstable DOCs near the critical

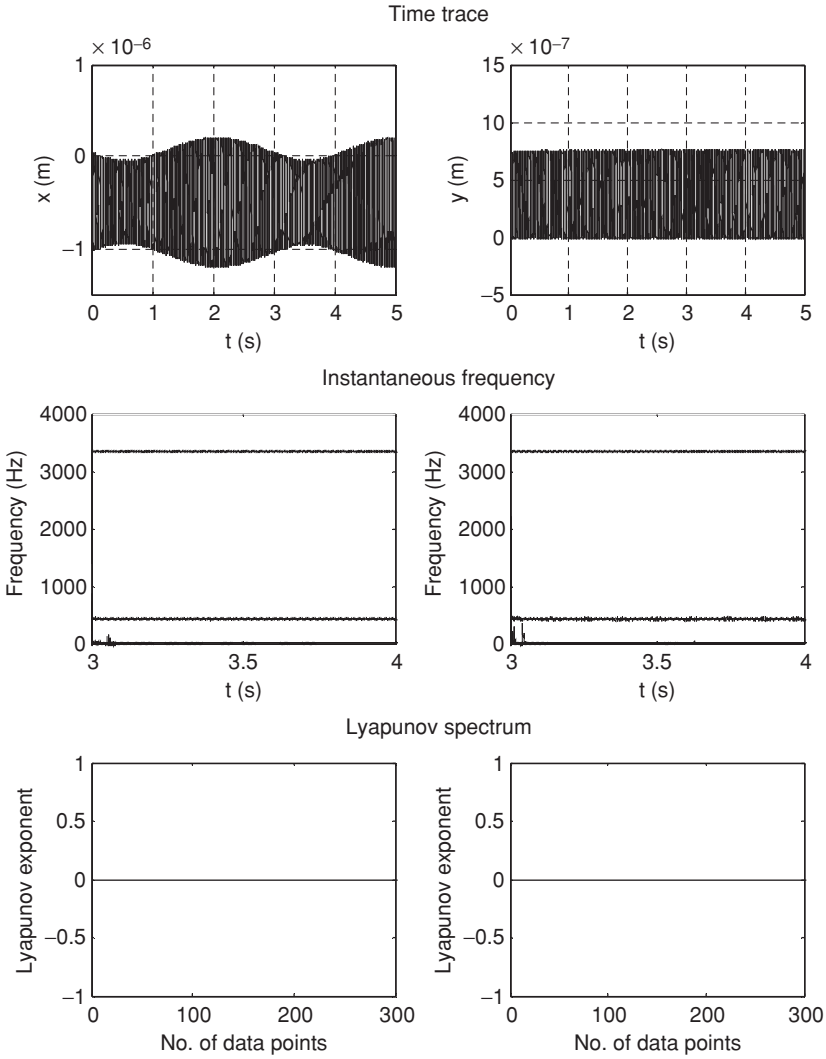

Figure 1.11 X-(left) and Y-(right) direction workpiece responses for DOC = 1.62 mm at $\Omega = 1000$ rpm

depth-of-cut are presented in the figures that follow. X- and Z-direction vibration responses are examined to identify the workpiece and tool stability margins respectively. Workpiece responses found in Figures 1.13, 1.14, 1.15, and 1.16, each illustrates a case of stability and a case of instability subject to two different DOCs at the same spindle speed. This is performed to identify the margin of instability for the particular DOCs considered.

Figure 1.13 shows the workpiece behaviors at close to the critical DOC at $\Omega = 750$ rpm. It is seen that the workpiece vibrates with stability subject to DOC = 1.40 mm, but becomes chaotic when DOC is increased to 1.45 mm at the same speed. Zero and positive Lyapunov

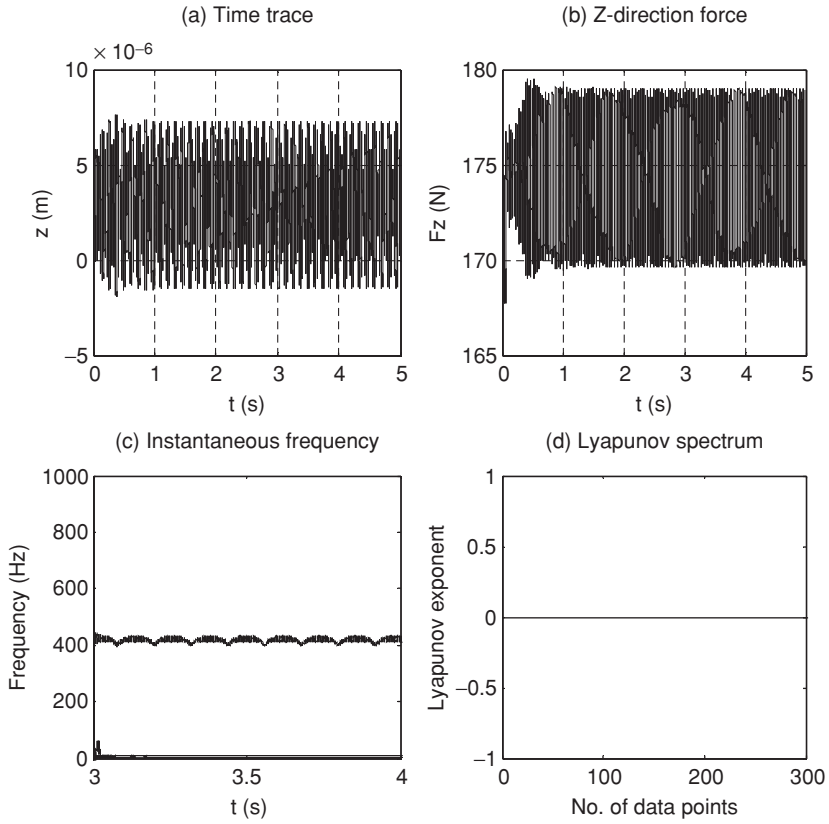

Figure 1.12 Z-direction tool behavior for DOC = 1.62 mm at $\Omega = 1000$ rpm

spectra clearly identify the two stages. The corresponding tool behavior is seen in Figure 1.17. The time traces show random oscillations once DOC is increased from 1.40 mm to 1.45 mm. The corresponding Lyapunov spectra confirm the same. The instantaneous frequency shows broadband characteristics in the lower frequency region for the stable case. The frequency excited by the tool natural frequency remains unvaried with time. Unlike the 1.40 mm case, when DOC is 1.45 mm the excited tool characteristic frequency varies in time. This frequency behavior can be seen in all the unstable plots of the tool in Figures 1.17, 1.18, 1.19, and 1.20 (right column) using large DOCs.

When speed is increased to 1000 rpm, the critical DOC also increases. Figure 1.14 shows the results of the workpiece vibrations corresponding to two different DOCs. It can be seen that the case corresponding to DOC = 1.75 mm is very stable in both the time and frequency domains. On the other hand, having a positive Lyapunov spectrum and broadband frequency characteristics, the case with DOC = 1.78 mm is an instability of chaos. The corresponding tool behaviors are found in Figure 1.18. Similar to the case with DOC = 750 rpm, violent oscillations, large vibration amplitudes, and a positive Lyapunov spectrum signify an unstable

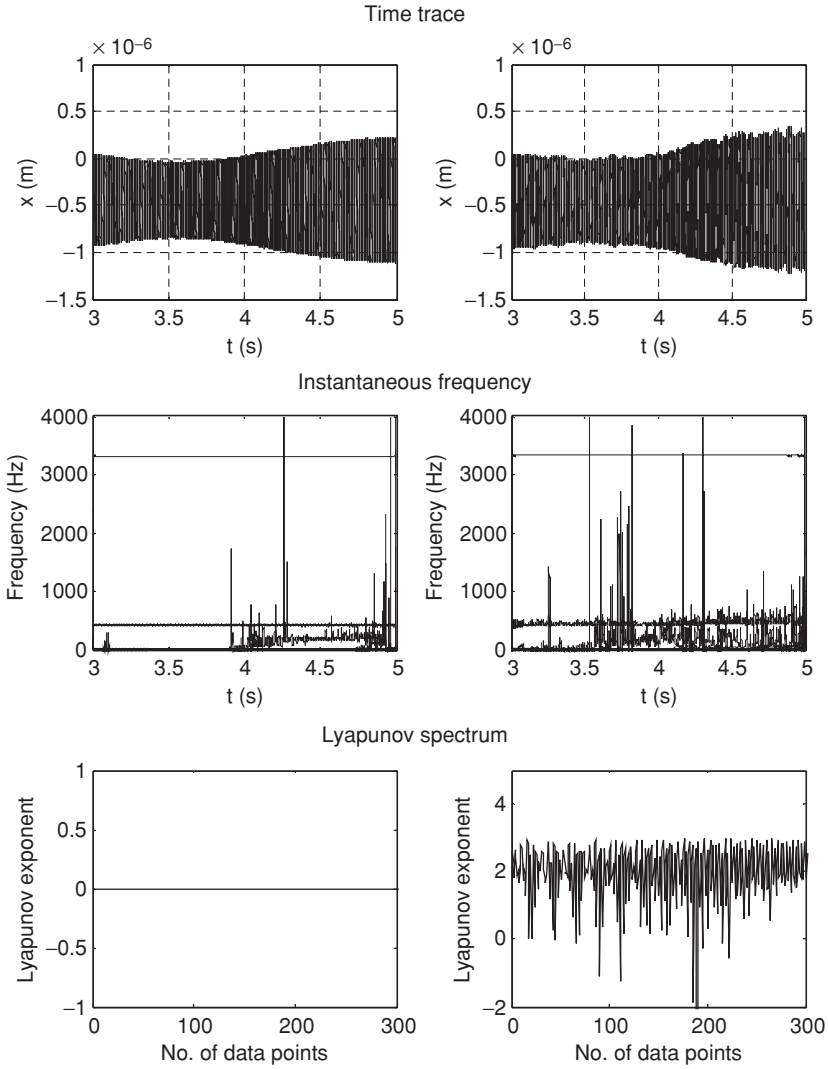

Figure 1.13 X-direction workpiece behavior for DOC = 1.40 mm (left) and DOC = 1.45 mm (right) at $\Omega = 750$ rpm

state of tool motion at DOC = 1.78 mm. Note that the response associated with the DOC is only 0.03 mm less than 1.78 mm, which is a case of stability.

Increasing the spindle speed further to 1250 rpm results in a stable state of cutting, thus moving the instability margin up to the 1.83–84 mm range (Fig. 1.15). Again, the associated time history, instantaneous frequency, and Lyapunov spectrum of the tool all indicate a state of chaos for DOC = 1.84 mm. This is in contrast with the case of DOC = 1.83 mm whose zero Lyapunov spectrum indicates stability. However, the time-frequency characteristics of

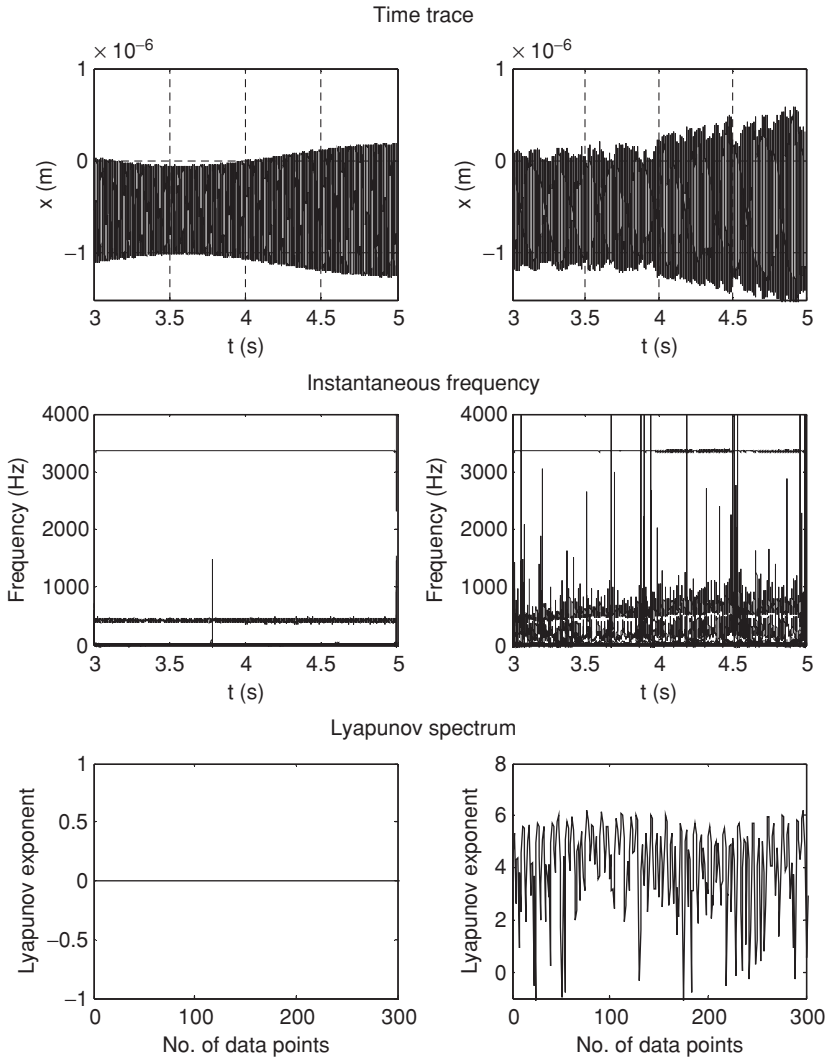

Figure 1.14 X-direction workpiece behavior for DOC = 1.75 mm (left) and DOC = 1.78 mm (right) at $\Omega = 1000$ rpm

the DOC = 1.83 mm case reveal that it is a bifurcated state. An increment of only one hundredth of a millimeter is enough to tip the stable cutting motion into dynamic instability. The tool responses in Figure 1.19 for the two DOCs convey a slightly different characteristic than the vibration results associated with the workpiece. Tool vibration amplitude is only several nanometers for the case with DOC = 1.83 mm. The 0.01 mm in increment induces chaotic responses of 0.1 mm in vibration amplitude. The state of chaotic motion is verified by the Lyapunov spectrum in Figure 1.19. Unlike all other cases considered, the instantaneous

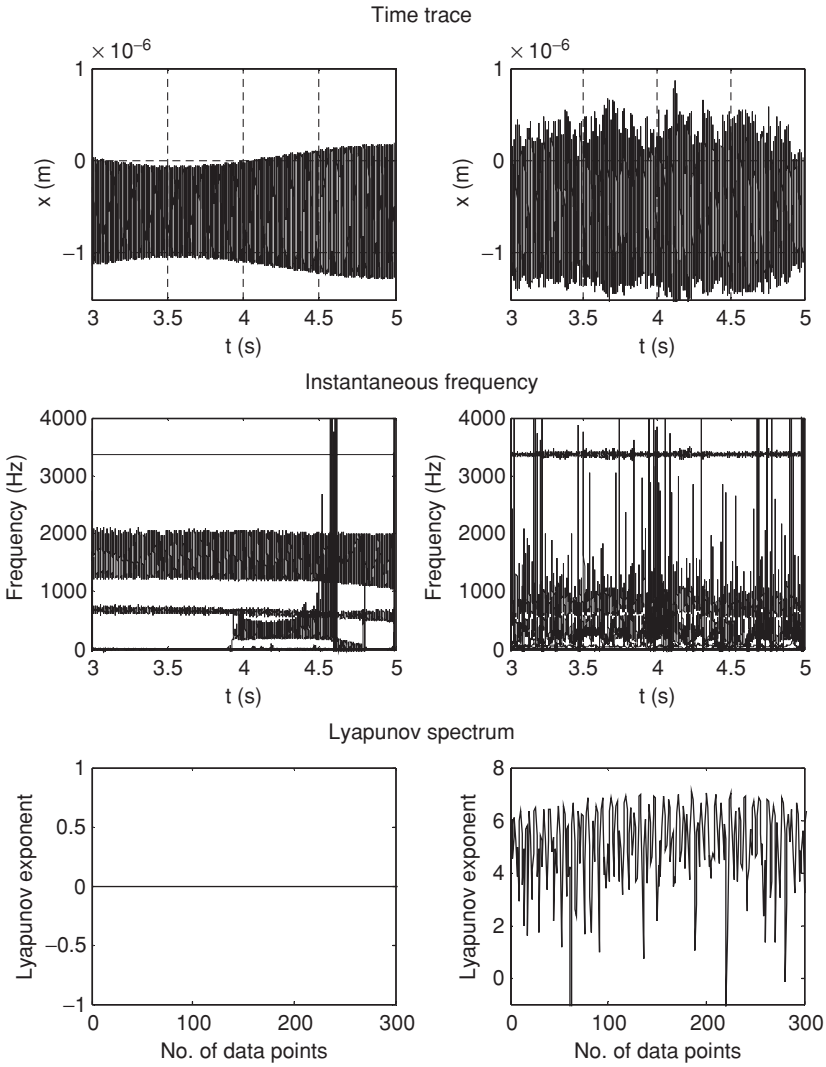

Figure 1.15 X-direction workpiece behavior for DOC = 1.83 mm (left) and DOC = 1.84 mm (right) at $\Omega = 1250$ rpm

frequency shows that the tool vibrates with a frequency closer to the workpiece natural frequency at the lower DOC. This frequency component immerges after 3.8 seconds. The Lyapunov spectrum of positive exponents for this case indicates that the motion is unstable.

Figure 1.16 shows the X-direction workpiece behaviors for DOC = 2.21 mm and 2.22 mm at $\Omega = 1500$ rpm. The time and frequency domain responses depict two different behaviors for the two DOCs. The Lyapunov spectrum for the lower DOC is not a straight line of zeros. It is an oscillation about zero, thus indicating that the motion is of a stable–unstable marginal

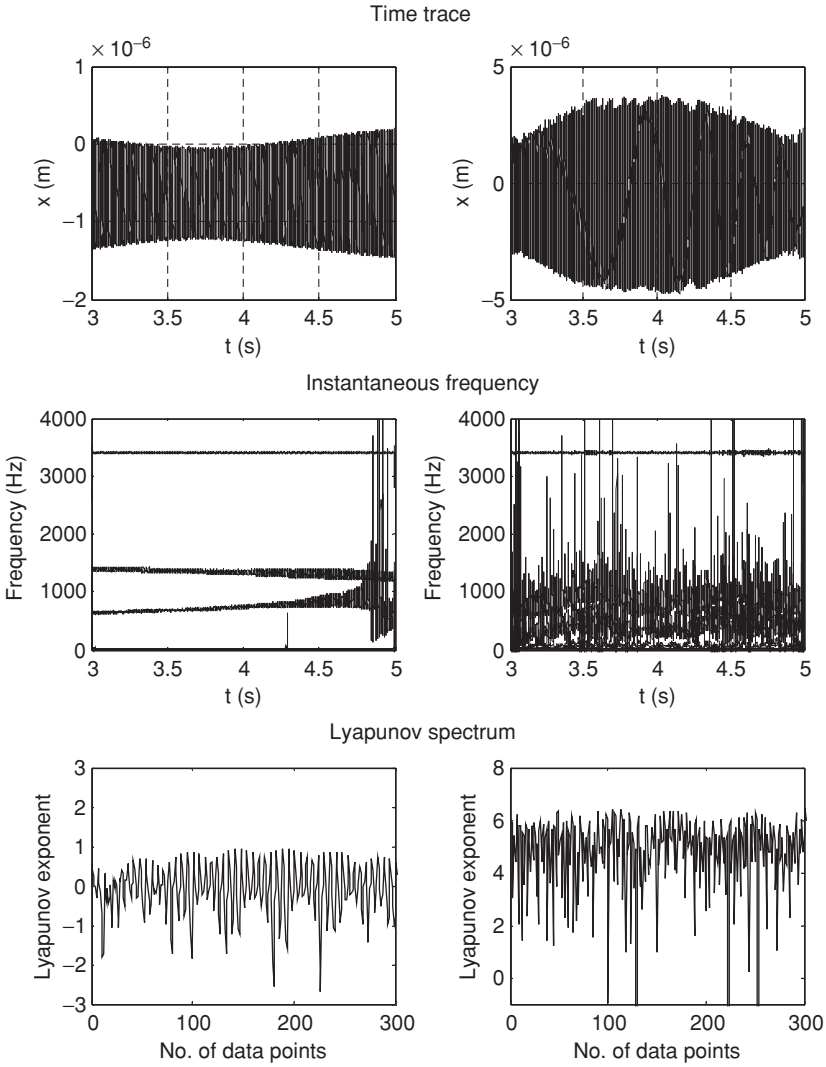

Figure 1.16 X-direction workpiece behavior for DOC = 2.21 mm (left) and DOC = 2.22 mm (right) at $\Omega = 1500$ rpm

type. The tool behavior at this speed is comparable to the case in Figure 1.20 where the speed was 1250 rpm. The vibration amplitude grows more than 10 000 times greater when DOC is increased by one hundredth of a millimeter from 2.21 mm to 2.22 mm. The instantaneous frequency for the lower DOC has a component of broadband characteristic at the workpiece natural frequency that appears after 3.5 seconds. The Lyapunov spectra for both DOCs are also positive, as is the case with $\Omega = 1250$ rpm. Using all the above cases of stable–unstable margin, the critical DOCs are determined for rough cutting at the various spindle speeds considered. Details will be given in the following section.

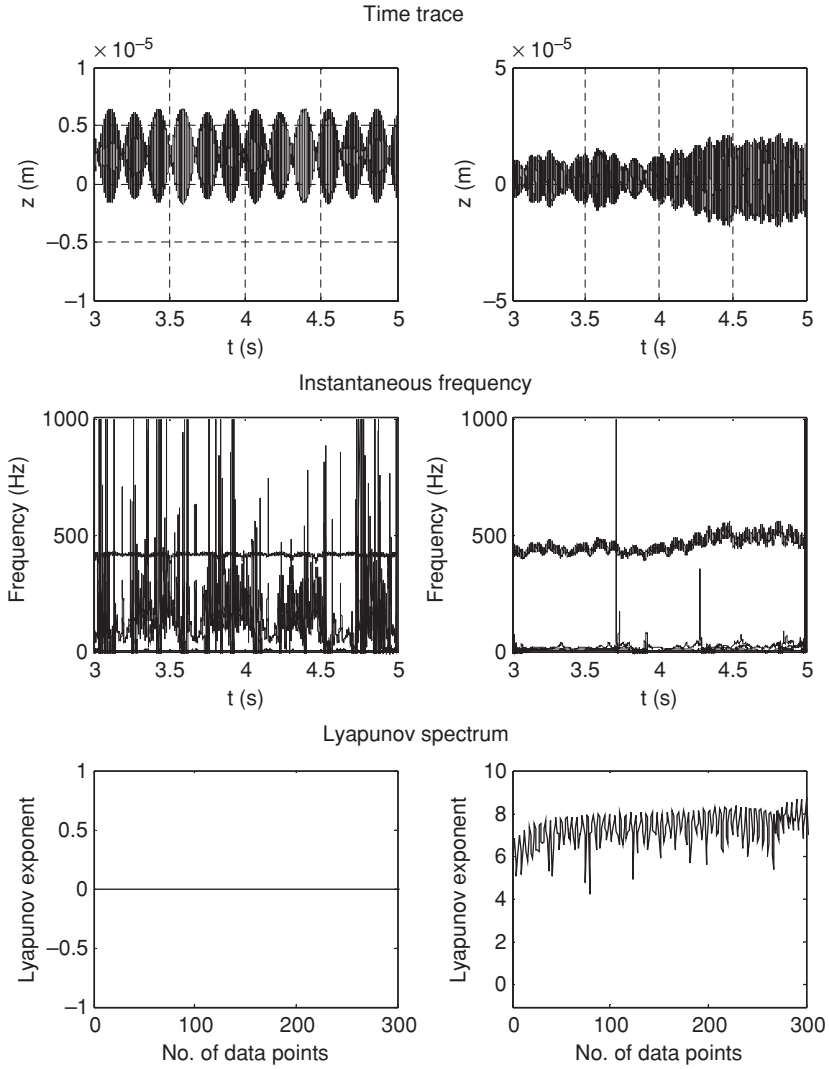

Figure 1.17 Z-direction tool behavior for DOC = 1.40 mm (left) and DOC = 1.45 mm (right) at $\Omega = 750$ rpm

Instead of spindle speed, cutting speed is the most common cutting parameter used in stability charts. For a workpiece having a machined section of D millimeters in diameter, the corresponding cutting speed is defined as follows

$$cutting\_speed = \frac{\pi D\Omega}{1000 \times 60}\ ms^{-1}$$

where Ω is spindle speed in revolutions per minute. This means that there can be different spindle speeds and workpiece diameters that have the same cutting speed. In milling or drilling,

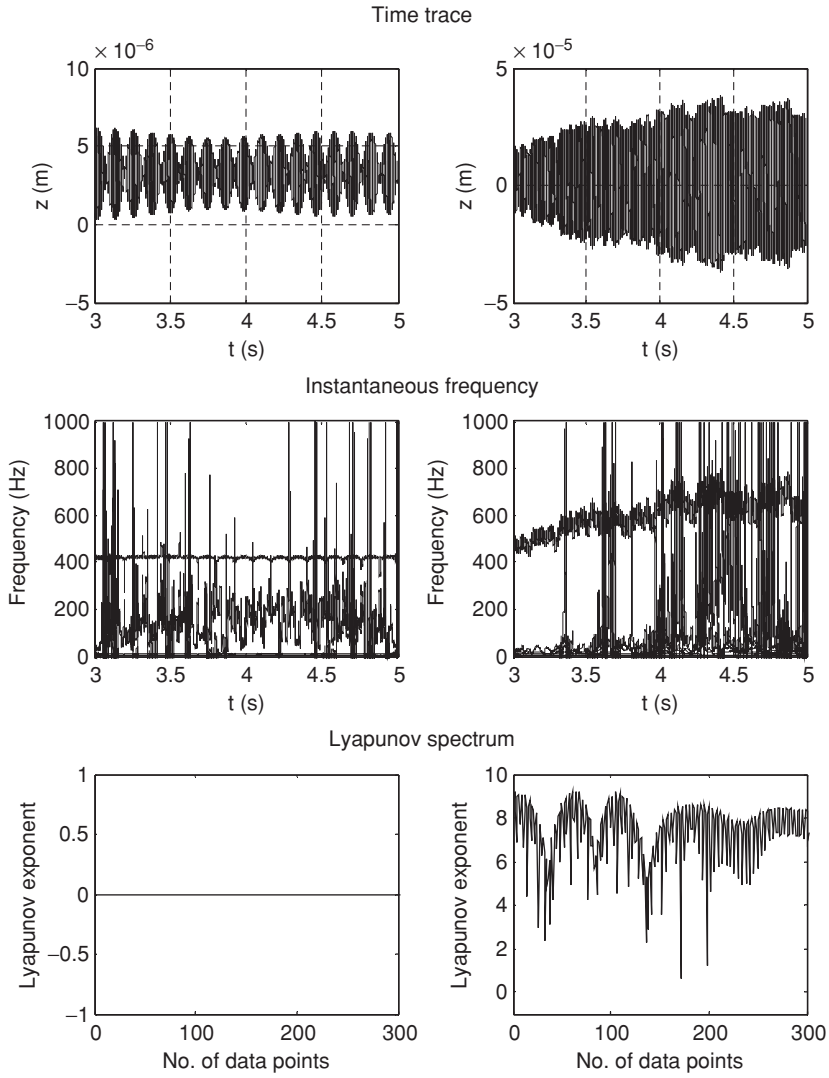

Figure 1.18 Z-direction tool behavior for DOC = 1.75 mm (left) and DOC = 1.78 mm (right) at $\Omega = 1000$ rpm

milling tools or drill bits have standard diameters. However, in turning processes, the machined diameter can be any value depending on the product requirements. The critical DOCs that were explored previously are compared with the experimental results in [7]. Experimentally found critical DOCs for cutting speeds in the range of 50 m/min to 300 m/min are published in [7].

Using the definition above, the stability limits can be presented as the critical DOC for each corresponding cutting speed as in Table 1.2.

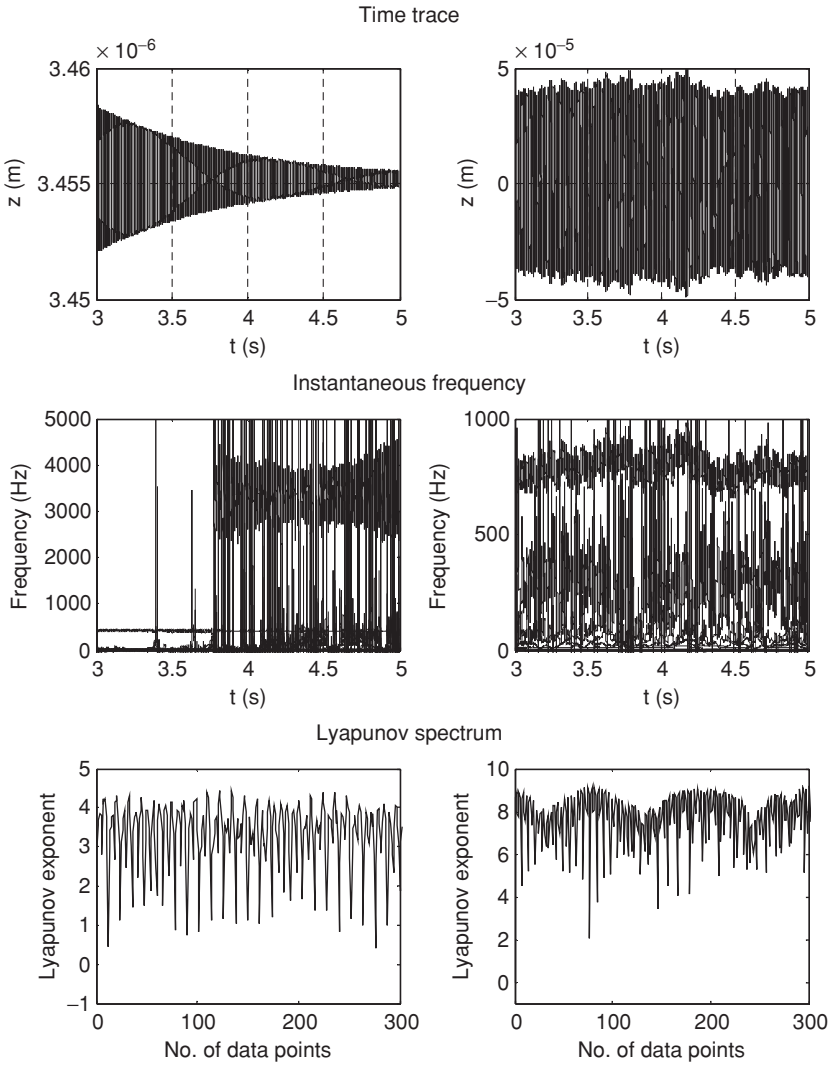

Figure 1.19 Z-direction tool behavior for DOC = 1.83 mm (left) and DOC = 1.84 mm (right) at $\Omega = 1250$ rpm

Table 1.2 Critical depth-of-cuts

Spindle speed (rpm)	Cutting speed (m/min)	Critical DOC (mm)
750	94.7	1.40–1.45
1000	126.3	1.75–1.78
1200	157.8	1.83
1500	189.4	2.21

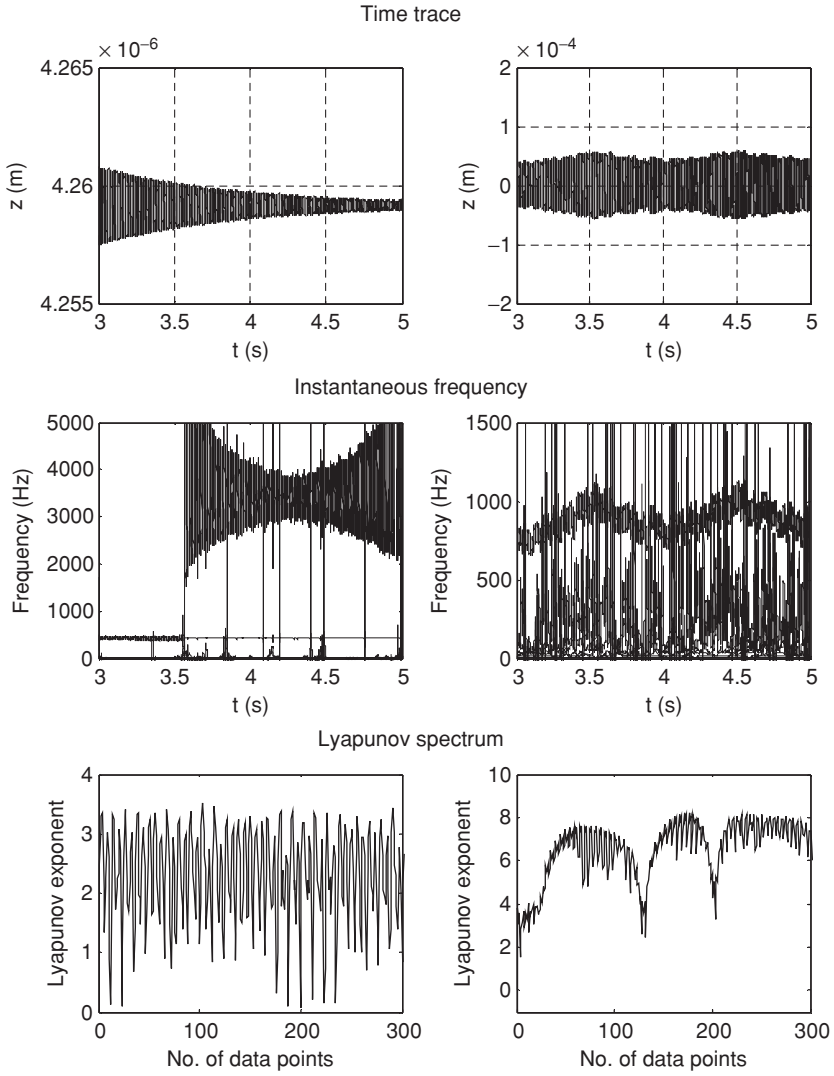

Figure 1.20 Z-direction tool behavior for DOC = 2.21 mm (left) and DOC = 2.22 mm (right) at $\Omega = 1500$ rpm

Figure 1.21 illustrates the comparison of critical DOCs with experimental results subject to increasing speeds. It should be mentioned that the experimental data were taken for a short workpiece and thus the stiffness of the workpiece was higher than the modeled workpiece considered in the section. It was established in previous sections that workpiece dimensions and tool geometry affect cutting stability. However, the workpiece dimensions and tool geometry used for the study are different from the corresponding experimental setup in [7]. Still, the feed rate employed herein differs only by about 5% from those experiments. These differences would certainly contribute to the differences in stability limits.

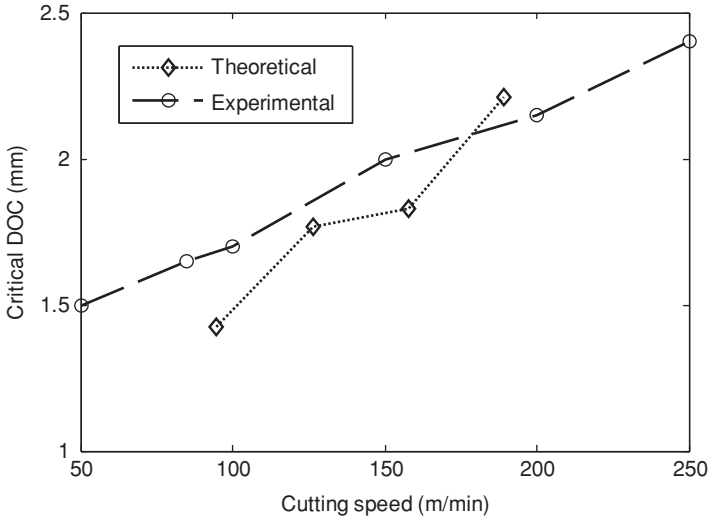

Figure 1.21 Comparison of critical DOC with experimental data

It should be noted that the experimental results in [7] are different from the conventional stability lobes for the ranges of speed that are considered here. Contrary to one's intuition, experiments have proved that critical DOC increases with cutting speed. The machining model also suggests the same.

1.4 Stability in Fine Cuts

Cutting stability subject to DOCs less than 1.00 mm is explored in this section. Three different DOCs at 0.50 mm, 0.75 mm, and 0.90 mm and four different spindle speeds at 750 rpm, 1000 rpm, 1250 rpm, and 1500 rpm are considered. The feed is 0.0965 mm for all cases. All figures have three columns for time traces, instantaneous frequencies, and Lyapunov spectrum. The four rows in the figures represent the results corresponding to four different speeds at a particular DOC.

The X-direction workpiece vibrations for fine cutting are considered below. Figure 1.22 shows the behavior of the case with DOC $= 0.50$ mm at four different speeds. Time traces for all the four speeds seem similar and their corresponding Lyapunov spectra all demonstrate instability with positive exponents. The workpiece is excited by the tool natural frequency in all cases, except for the case at $\Omega = 1250$ rpm.

When DOC is increased to 0.75 mm, the workpiece becomes more stable in Figure 1.23. Similar to the case with DOC $= 0.50$ mm, increasing spindle speed does not significantly alter the stability state of the workpiece for DOC $= 0.75$ mm. All instantaneous frequency plots have a broad bandwidth component at 850–900 Hz. This might be explained by the frequency-doubling of the tool natural frequency. In addition, the Lyapunov spectra do not indicate clean-cut stability with zero exponents. But rather the exponents oscillate near zero

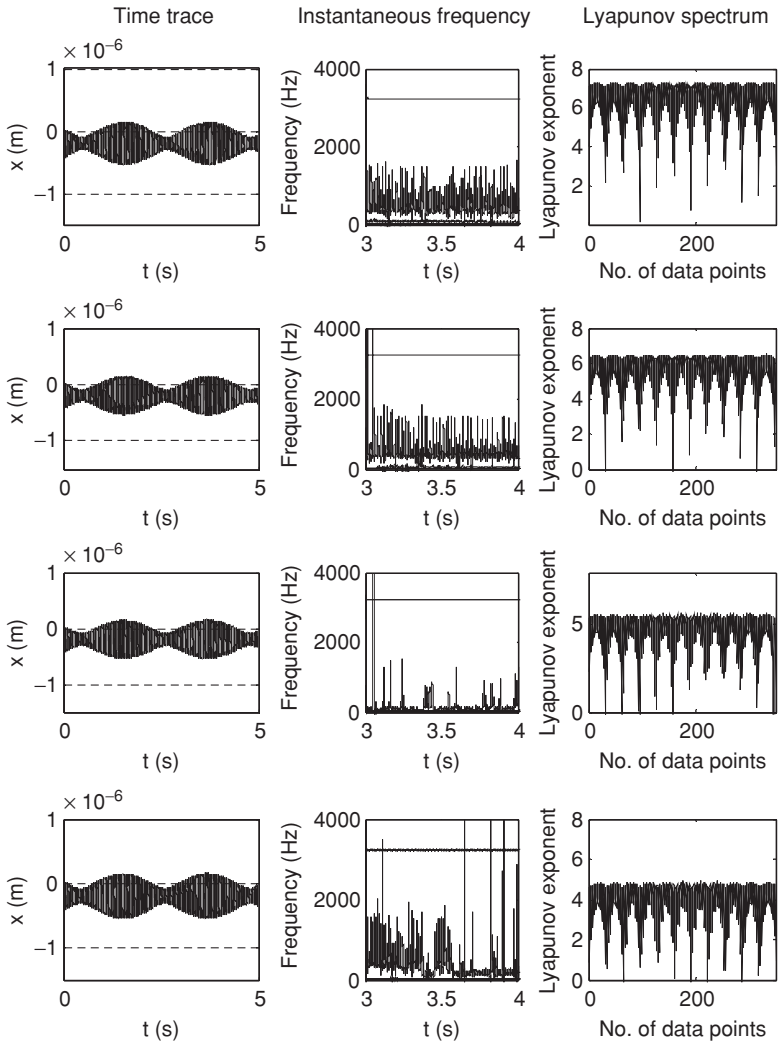

Figure 1.22 X-direction workpiece behavior for DOC = 0.50 mm at (a) $\Omega = 750$ rpm (1st row), (b) $\Omega = 1000$ rpm (2nd row), (c) $\Omega = 1250$ rpm (3rd row), and (d) $\Omega = 1500$ rpm (4th row)

and towards the negative side of the spectra. This can be considered a marginal stable–unstable situation of the workpiece.

Figure 1.24 demonstrates the workpiece behavior subject to DOC = 0.90 mm. It can be seen that the workpiece is in a stable state of motion at this DOC. All the four instantaneous frequency plots illustrate similar types of bifurcated situation having whirling frequency and components other than the workpiece natural frequency. In all cases shown in Figure 1.24, one frequency is between 450–600 Hz and the other extra component is in the range of 1300–1400 Hz. These frequency components do not vary with time or display broadband behaviors.

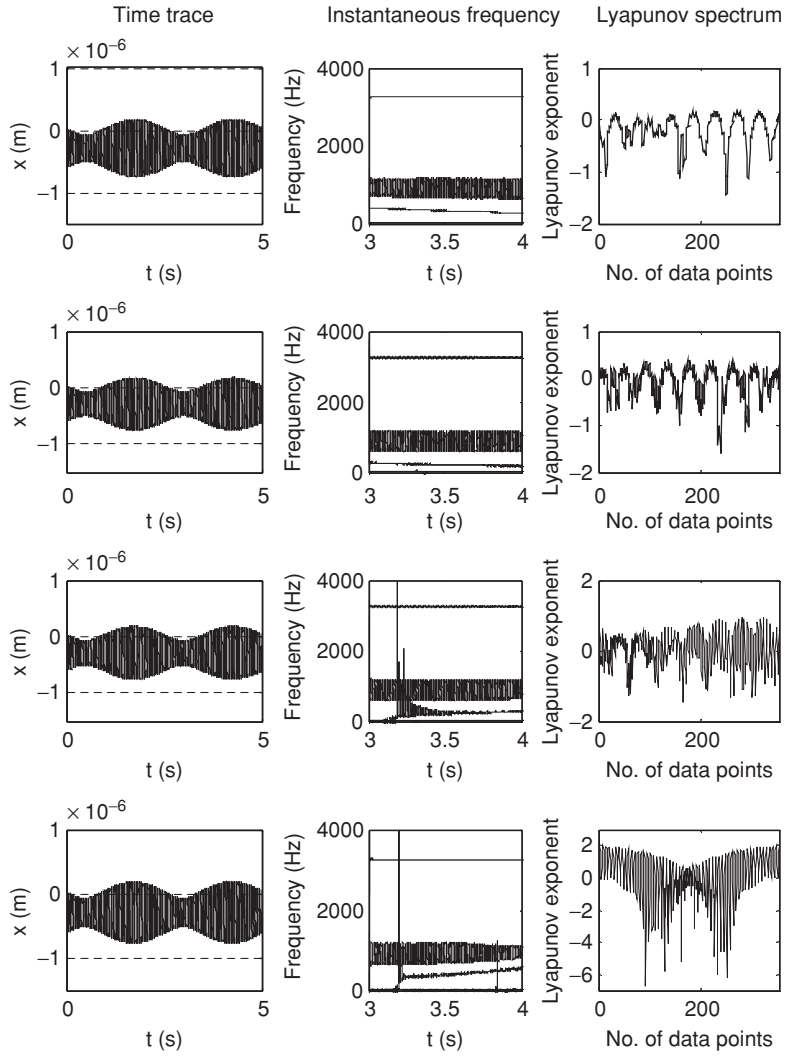

Figure 1.23 X-direction workpiece behavior for DOC = 0.75 mm at (a) Ω = 750 rpm (1st row), (b) Ω = 1000 rpm (2nd row), (c) Ω = 1250 rpm (3rd row), and (d) Ω = 1500 rpm (4th row)

The motion is periodic and stable, as is verified by the zero Lyapunov spectra. It is interesting to note that regardless of the speed in the range considered, the workpiece is dynamically unstable at DOC = 0.50 mm. But it is marginally stable at DOC = 0.75 mm and stable at DOC = 0.90 mm.

The tool stability in the Z-direction investigated in this section considers both time and time-frequency analysis as in the previous sections. Figure 1.25 shows the tool behavior at DOC = 0.50 mm. It is noted that except for the 1250 rpm case, all time traces look similar. In addition, the corresponding instantaneous frequency plots also show the same similarity having bifurcations only in the low frequency region without indicating any broadband behavior.

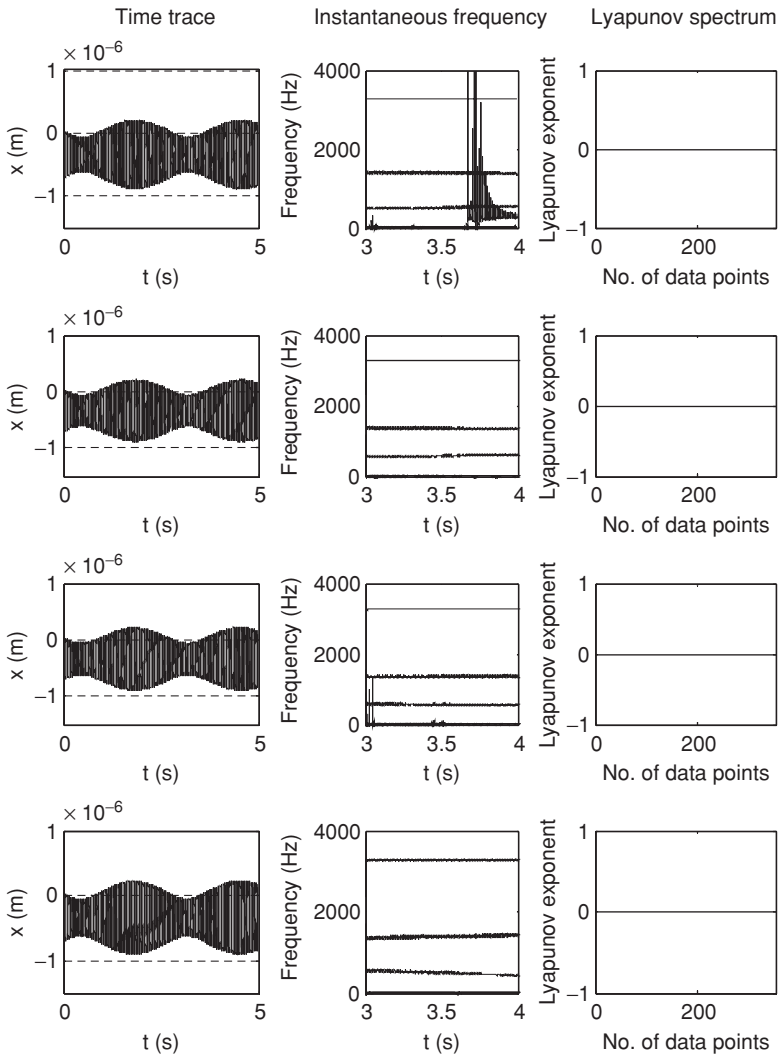

Figure 1.24 X-direction workpiece behavior for DOC = 0.90 mm at (a) $\Omega = 750$ rpm (1st row), (b) $\Omega = 1000$ rpm (2nd row), (c) $\Omega = 1250$ rpm (3rd row), and (d) $\Omega = 1500$ rpm (4th row)

When spindle speed is 1250 rpm in Figure 1.25(c), the tool is excited by the workpiece natural frequency and displays broadband characteristics. Moreover, the associated Lyapunov spectrum indicates an unstable condition, while in all other cases the tool motion is stable with zero exponents.

When DOC is increased to 0.75 mm, all speed cases display similar characteristics having very small vibration amplitudes and bifurcations in the instantaneous frequency plots in Figure 1.26. However, all Lyapunov spectra demonstrate stable behaviors with zero exponents. Increasing DOC further to 0.90 mm, two categories out of the four different speeds in

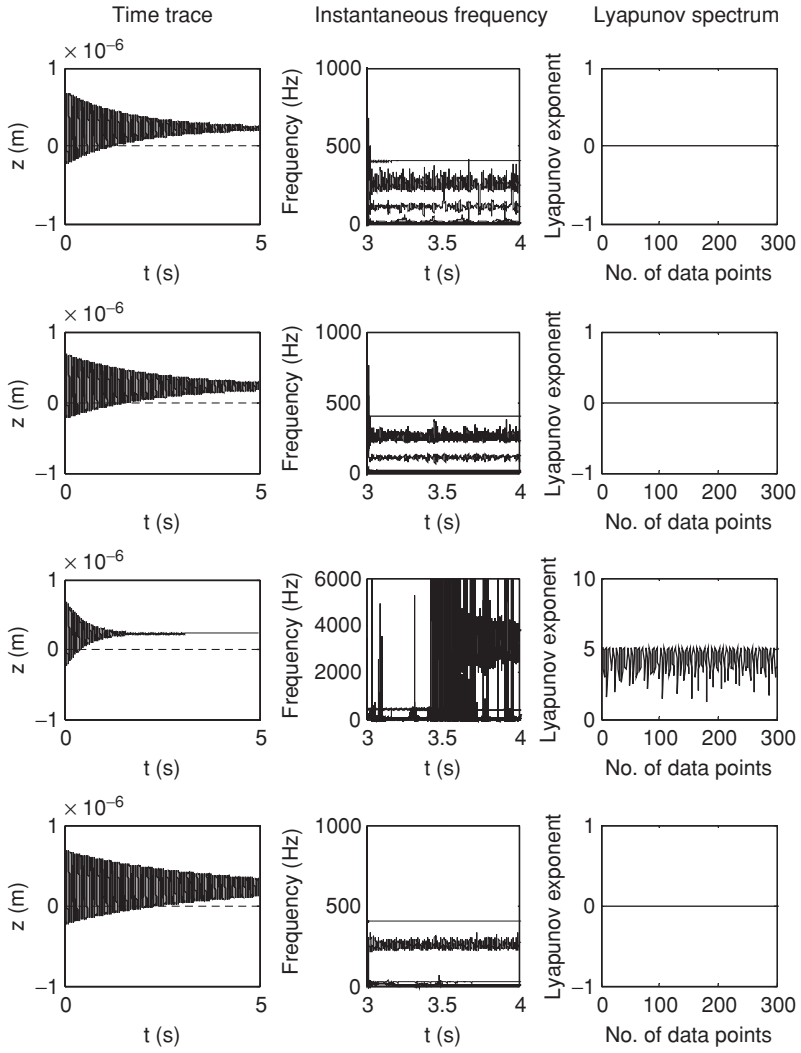

Figure 1.25 Z-direction tool behavior for DOC = 0.50 mm at (a) $\Omega = 750$ rpm (1st row), (b) $\Omega = 1000$ rpm (2nd row), (c) $\Omega = 1250$ rpm (3rd row), and (d) $\Omega = 1500$ rpm (4th row)

Figure 1.27 are seen. The 750 rpm and 1250 rpm cases are alike, while the 1000 rpm and 1500 rpm cases are comparable. Lyapunov spectra show that the 750 rpm and 1250 rpm cases are unstable, and the other two speed cases are stable. Many frequency components are also present in the 1000 rpm and 1500 rpm cases, despite the fact that the system is stable according to the Lyapunov spectrums in Figure 1.28.

Overall system stability can now be determined by examining the stable and unstable situations of the workpiece and the tool. The system is stable if both workpiece and tool demonstrate stable situations. If either of them displays instability, the system is unstable.

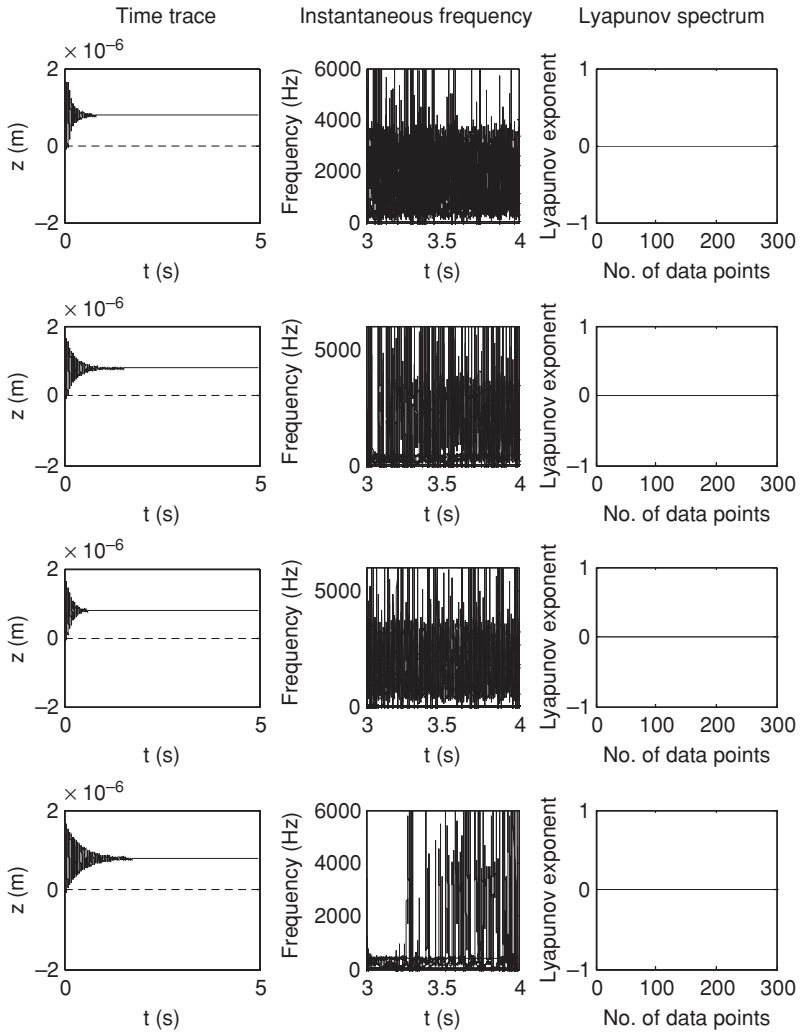

Figure 1.26 Z-direction tool behavior for DOC = 0.75 mm at (a) Ω = 750rpm (1st row), (b) Ω = 1000 rpm (2nd row), (c) Ω = 1250 rpm (3rd row), and (d) Ω = 1500 rpm (4th row)

Using this classification, system stability can be summarized as in Table 1.3 below. Here the notions US, S, and MS stand for Unstable, Stable, and Marginally Stable, respectively. Since the workpiece is unstable for all the speeds at DOC = 0.50 mm, the system is unstable for the DOC. Moreover, the workpiece demonstrates a stable–unstable situation for all four speeds considered and the tool shows highly bifurcated situations for all the cases when DOC = 0.75 mm, thus making the system marginally stable. On the other hand, even though the workpiece is stable at DOC = 0.90 mm for all four speeds, the tool is unstable for the 750 rpm and 1250 rpm cases. Thus the system is one of instability for these two cases.

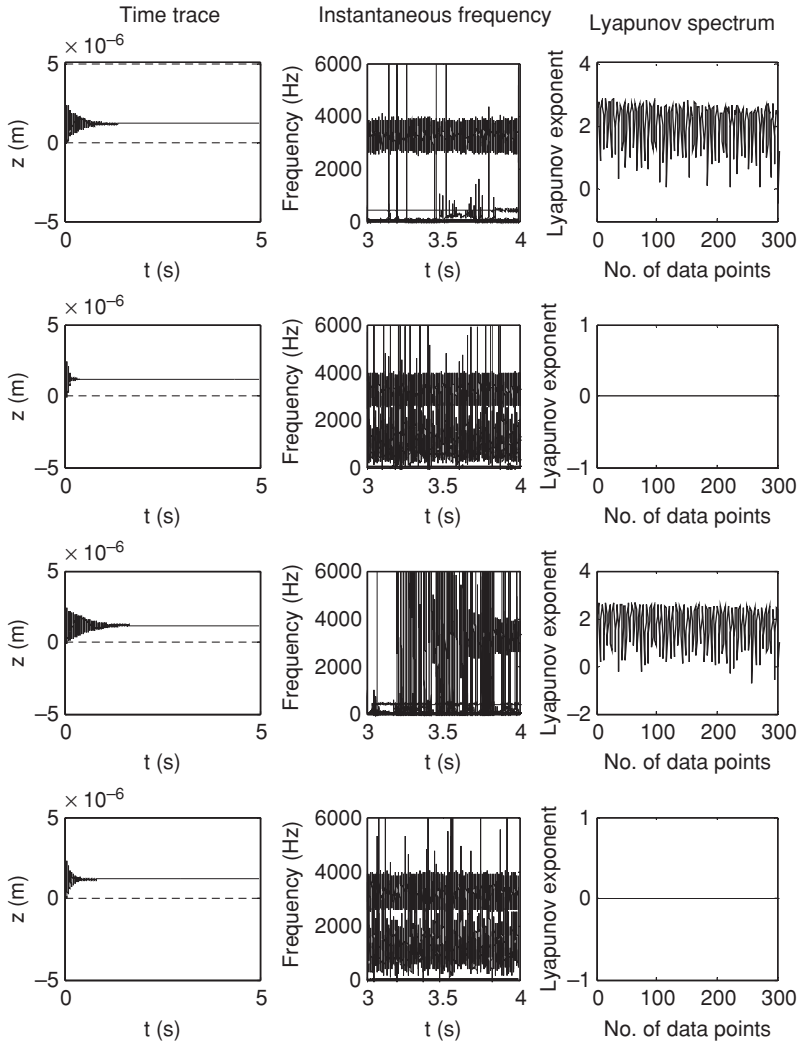

Figure 1.27 Z-direction tool behavior for DOC = 0.90 mm at (a) Ω = 750 rpm (1st row), (b) Ω = 1000 rpm (2nd row), (c) Ω = 1250 rpm (3rd row), and (d) Ω = 1500 rpm (4th row)

Table 1.3 System stability

	Spindle speed (rpm)			
DOC (mm)	750	1000	1200	1500
0.90	US	S	US	S
0.75	MS	US	MS	US
0.50	US	MS	US	MS

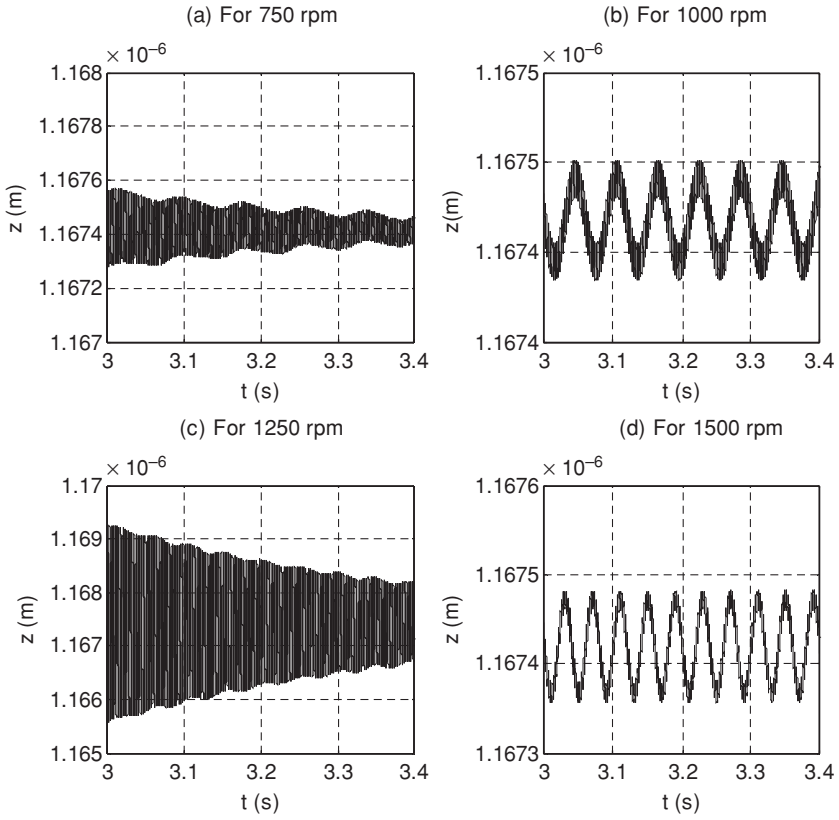

Figure 1.28 Time traces for tool vibrations between 3.0 and 3.4 seconds for 0.90 mm DOC

Study of machining stability for rough cuts suggests that, for the speed range considered, low speeds impart instability. However, bifurcated states could be staged in between with increasing speeds. Therefore it cannot be concluded that speed increase will always result in stability. Using the presented turning model, critical DOCs, on the other hand, were seen to increase with the increase of speed. It was shown that this observation was consistent with experimental data. It was noted that cutting force amplitude oscillations were determined by the nonlinearity of the force, not by speed increments. It was also seen that both the tool and workpiece showed similar instability stages most of the time. However, when it was closer to the critical depth-of-cut, the cutting tool reached instability before the workpiece did. In contrast to this observation, when DOC is less than 1.00 mm, most of the time when the system was unstable, only the workpiece or the tool was unstable and not both. There were a few situations where both became unstable at the same time. It was noted that in all cases where the tool was unstable, the tool was excited by the workpiece natural frequency and displayed broadband behavior. However, not all cases in which the tool was excited by the workpiece natural frequency were unstable. On the other hand, in almost all cases in which the workpiece was unstable, the workpiece had a broadband frequency component near the tool

natural frequency. This suggests the importance of considering the workpiece–tool coupling effect in modeling cutting dynamics.

1.5 Concluding Remarks

The three-dimensional, nonlinear dynamic model incorporated *regenerative effect*, *cutting force nonlinearity*, *tool nonlinearity*, *imbalance-induced whirling, and mass and stiffness reduction of the workpiece* to realize simultaneous coupled tool–workpiece vibrations. Model responses subject to whirling were examined for various cases of cutting parameters including depth-of-cut, spindle speed, feed rate, and tool geometry. Stability analysis was performed using instantaneous frequency and Lyapunov spectrum. The following can be summarized based on the results discussed and observations made in the previous sections:

- Concerns over several major issues were raised. It was concluded that workpiece vibrations in modeling turning operation cannot be neglected. The significance of whirling and tool nonlinearity cannot be ignored.
- The various responses of the 3D machining model were shown to agree favorably with experimental data available in the literature.
- Negligence of workpiece vibrations will result in physically inadmissible results.
- Workpiece dimensions impact cutting stability in a non-negligible way.
- Workpiece–tool coupling is significant for the proper interpretation of tool dynamics.
- Use of linearized models for studying cutting dynamics will inevitably generate erroneous, unreliable information.
- Whirling was found to contribute to machining stability and larger workpiece vibration amplitude.

Whirling will affect tool dynamics only when high feed rates are considered. When the critical depth-of-cut is reached and the workpiece vibrates with instability, whirling becomes negligible. Consideration of nonlinearity in modeling machining processes is crucial for understanding the underlying cutting dynamics. Tool geometry significantly affects cutting stability. Machining models disregarding tool geometry will miscomprehend cutting response. Feed rate has an impact on cutting stability. A high feed rate could impart stability to fine turning operation. However, more elaborated investigations are needed to prove that high feed rate does contribute to higher stability limits.

Critical DOC increases with increasing spindle speed. This observation agrees well, in the qualitative sense, with available physical data. Modeling results supported the idea that chatter could occur at low DOCs. This is in agreement with what [8] suggests and what [7] observes in testing. Thus, unlike conventional stability charts, the stability limits established in the chapter have both upper and lower stability regions.

The stability margin for rough cuts using large DOCs can be separated by a line. However, for fine cuts using smaller DOCs there are different stability regions and no stability limits.

Machining chatter can be associated with one of the four types of dynamic stability–instability scenarios: (1) both tool and workpiece are stable, (2) the tool is stable when the workpiece is unstable, (3) the workpiece is stable when the tool is unstable, and (4) both tool and workpiece are unstable.

References

[1] Huo, D., Cheng, K., 2008, "A Dynamics-Driven Approach to The Design of Precision Machine Tools for Micro-Manufacturing and Its Implementation Perspectives," *Proceedings of the Institution of Mechanical Engineers, Part B: Journal of Engineering Manufacture*, 222(1), 1–13.

[2] Dassanayake, A.V., Suh, C.S., 2007, "Machining Dynamics Involving Whirling. Part I: Model Development and Validation," *Journal of Vibration and Control*, 13(5), 475–506.

[3] Dassanayake, A.V., Suh, C.S., 2007, "Machining Dynamics Involving Whirling. Part II: Machining States Described by Nonlinear and Linearized Models," *Journal of Vibration and Control*, 13(5), 507–26.

[4] Dassanayake, A.V., Suh, C.S., 2008, "On Nonlinear Cutting Response and Tool Chatter in Turning Operation," *Communications in Nonlinear Science and Numerical Simulations*, 13(5), 979–1001.

[5] Dassanayake, A.V., 2006, Machining Dynamics and Stability Analysis in Longitudinal Turning Involving Work-piece Whirling, PhD Dissertation, Texas A&M University.

[6] Rao, B. C., Shin, Y. C., 1999, "A Comprehensive Dynamic Cutting Force model for Chatter Prediction in Turning," *International Journal of Machine Tools and Manufacture*, 9(10), 1631–54.

[7] Kim, J.S., Lee, B.H., 1990, "An Analytical Model of Dynamic Cutting Forces in Chatter Vibration," *International Journal of Machine Tools and Manufacture*, 31(3), 371–81.

[8] Volger, M. P., DeVor, R. E., Kapoor, S. G., 2002, "Nonlinear Influence of Effective Lead Angle in Turning Process Stability," *ASME Journal of Manufacturing Science and Engineering*, 124(2), 473–75.